Heterogeneous Structure, Heterogeneous Dynamics, and Complex Behavior in Two-Dimensional Liquids

ARTICLE *in* JOURNAL OF PHYSICAL CHEMISTRY LETTERS · SEPTEMBER 2012

Impact Factor: 7.46 · DOI: 10.1021/jz301006j

5 AUTHORS, INCLUDING:

Alexander Patashinski
Northwestern University
58 PUBLICATIONS **432** CITATIONS

SEE PROFILE

Mark A. Ratner
Northwestern University
906 PUBLICATIONS **42,483** CITATIONS

SEE PROFILE

Rafal Orlik
Orlik Software
17 PUBLICATIONS **54** CITATIONS

SEE PROFILE

Melting in 2D Lennard-Jones Systems: What Type of Phase Transition?†

Alexander Z. Patashinski,*,‡,# Rafal Orlik,§ Antoni C. Mitus,⊥ Bartosz A. Grzybowski,‡,# and Mark A. Ratner‡

Department of Chemistry, Northwestern University, 2145 Sheridan Road, Evanston, Illinois 60208-3113, Orlik Software, ul. Lniana 22/12, 50-520 Wrocław, Poland, Institute of Physics, University of Technology, Wybrzeze Wyspianskiego 27, 50-370 Wroclaw, Poland, and Department of Chemical and Biological Engineering, Northwestern University, 2145 Sheridan Road, Evanston, Illinois 60208-3113

Received: July 26, 2010; Revised Manuscript Received: September 1, 2010

A typical configuration of an equilibrium 2D system of 2500 Lennard-Jones particles at melting is found to be a mosaic of crystallites and amorphous clusters. This mosaic significantly changed at times around the period τ of local vibrations, while most particles retain their nearest neighbors for times much longer than τ. In a system of 2500 particles, we found no phase separation for length scales larger than that of a crystallite. With decreasing density, the number of small amorphous clusters increased, and proliferation and percolation of amorphous matter separated the crystalline-ordered parts so that correlations between local order orientations of remote crystallites disappeared. We suggest that the mosaic is a manifestation of diminished stability of the crystalline structure resulting from competition between attraction and repulsion forces.

1. Introduction

To explain melting in two-dimensional (2D) systems,[1−32] two different scenarios were suggested, defect−agglomeration (amorphyzation) melting (see the review in ref 2) via a discontinuous phase transition and the dislocation−unbinding scenario proposed by Nelson and Halperin, often referred to as the BKTHNY (Berezinsky−Kosterlitz−Thouless−Nelson−Halperin−Young) theory.[1,3−8] The main prediction of this theory is a continuous melting into a hexatic liquid characterized by an algebraic decay of orientation correlations. The data to test the theories were mostly obtained by computer simulations of 2D Lennard-Jones (LJ) and other systems.[3,9−33] In these simulations, both the number of particles N and the simulation time were rather small compared to those of experiments with real systems. Using the results of simulations to understand 2D melting in the macroscopic limit is always an extrapolation that needs further justification.

Earlier simulations dealt with particle numbers $N < 10^4$ and simulation times limited to hundreds and even tens of particle vibration periods τ. A list of references and the overview of the results of these early studies can be found in reviews in refs 1−3. In ref 2, data for LJ and other systems were interpreted in terms of a discontinuous (first-order) defect−agglomeration phase transition, with the phase diagram shown in Figure 1. Defect−agglomeration refers to a general idea of spontaneous appearance of amorphous regions that break up the global order in the system; a possibility to describe the amorphous region in terms of simpler defects is an additional assumption that is not usually necessary. A rather general model of defect−agglomeration (amorphyzation) melting was discussed in ref 34; the main suggestion of this model is the existence of several preferred arrangements (inherent structures) in a small cluster.

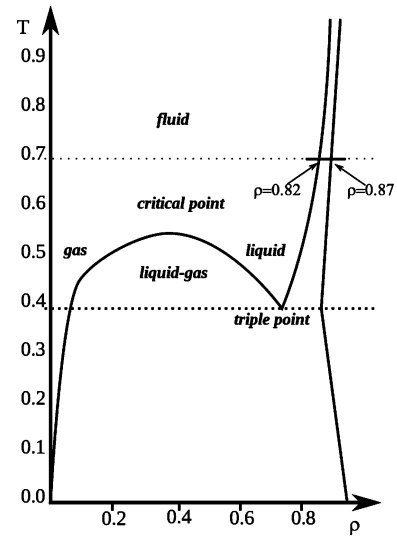

Figure 1. Phase diagram of 2D LJ system in reduced variables $T - \rho$ (adapted from ref 38).

More recent studies of 2D melting[35−37] used very long simulation times in large ($N \approx 10^5$) systems. Simulations[35,36] of LJ crystals close to the melting point found a power law decrease of orientation correlations consistent with the predictions of the BKTHNY theory. However, close to the expected continuous dislocation−unbinding transition, the unbinding regime was interrupted by a spontaneous jump from crystalline-ordered to a liquid state, with a possible transient appearance of a hexatic liquid in the overheated crystal. No equilibrium hexatic liquid was found above melting. In some contrast to these findings, for a system of particles interacting via only the repulsive part of the LJ interaction, a continuous transition from an equilibrium liquid to an equilibrium hexatic liquid was found

† Part of the "Mark A. Ratner Festschrift".

* To whom correspondence should be addressed. E-mail: a-patashinski@northwestern.edu.

‡ Department of Chemistry, Northwestern University.

§ Orlik Software.

⊥ University of Technology.

Department of Chemical and Biological Engineering, Northwestern University.

▽ E-mail: rafal.orlik@orlik-software.eu (R.O.); antoni.mitus@pwr.wroc.pl (A.C.M.); grzybor@northwestern.edu (B.A.G.); Ratner@chem.northwestern.edu (M.A.R.).

10.1021/jp1069412
Published on Web 09/22/2010

upon heating.[37] One may conclude from these data that the attraction part of the LJ potential is responsible for an instability of the system leading to a discontinuous transition. The objective of this study is to examine possible mechanisms of this instability.

We note that in microscopic theory, both the dislocation−unbinding and the amorphyzation melting scenarios are approximations based on special selections of particle configurations accounted for in the corresponding theory. The BKTHNY theory ignores phonon (sound waves) degrees of freedom and considers an ideal lattice hosting dislocation. The theory describes continuous changes in the orientation long-range order; for finite distances, correlations are continuous at the transition temperature. In contrast to the unbinding scenario, the defect−agglomeration approach assumes proliferation and a discontinuous jump in the fraction of the system occupied by noncrystalline clusters.

Data about thermodynamic and binary correlation functions can only give an indirect test of the assumptions underlying specified scenarios. A direct proof assumes analyzing typical configurations of the system at and close to the phase transition. Here, "typical" means that configurations with similar features appear with high probability while configurations with significantly different features have negligibly low probabilities. In particular, critical for the dislocation−unbinding scenario is an unambiguous definition of bonds orientations in small parts of the system. Large fluctuations of bond orientations near the melting temperature, found in refs 3, 39, and 40, can make the definition of local orientation ambiguous.

In this paper, we study the space distribution of order and disorder in a typical configuration of a $N = 2500$ particle system at melting. The system was simulated along the supercritical isotherm $T = 0.7$ (in reduced temperature units). We colored particles depending on the degree of order in their near environments. This visualization revealed unexpected features of typical configurations, absence of detectable macroscopic phase separation and a granular, microphase-separated structure. A typical configuration was found to be a mosaic of small (∼10−50 particles) crystallites separated by less-ordered amorphous regions of similar size. The total fraction of crystallites did not fluctuate abnormally, but the space distribution of crystallites and amorphous regions substantially changed at times on the order of the period τ of particle vibrations. However, for most particles, their six nearest neighbors remained unchanged for much longer times.

In the following, we describe the methods used in this study and their application and then discuss the melting scenarios in relation to the results of this study.

2. The System

The 2D system of $N = 50 \times 50 = 2500$ LJ particles was simulated under periodic boundary conditions. Below, we use reduced units[2,41] for energy (ε), length (σ), and time (τ). In these units, the potential energy of the system has the form

$$U\{r^{(a)}\} = \frac{1}{2}\sum_{b,b'=1}^{N} U_{\mathrm{LJ}}(|r^{(b)} - r^{(b')}|)$$

$$U_{\mathrm{LJ}}(r) = 4\left[\left(\frac{1}{r}\right)^{12} - \left(\frac{1}{r}\right)^{6}\right] \quad (1)$$

Here, $a = 1, ..., N$ labels particles; $r^{(a)}$ are the Euclidian coordinates of particle a. N is the number of particles in a square-shaped region of size L and "volume" $V = L^2$. The particle number density is $\rho = N/V$. The critical temperature for the system (1) is $T_c \approx 0.55$;[2] the unit of time $\sigma(M/(48\varepsilon))^{1/2}$ is related to the mass M of a particle and is of the same order as the period τ of the particle's thermal vibrations.

The melting range of densities (see Figure), $\rho = 0.78-0.94$, was scanned along the supercritical isotherm $T = 0.7$. A standard molecular dynamics (MD) method with velocity Verlet algorithm (see, for example, ref 41) was used. The time step h was chosen to be $h = 0.0064$ in the LJ time units; this choice approximately corresponds to $\tau = 500h$. We used (*NVT*) (constant particle number N, volume V, and temperature T) simulations at the equilibration and relaxation part of the simulation (usually first 5×10^4 steps) and then (*NVT*) or (*NVE*) (constant N, V, and energy E) simulations during sampling. The velocity Verlet algorithm is known for good conservation of the energy, and we observed no measurable self-heating or -cooling of the system and no recognizable differences between properties of typical configurations between these ensembles.

Starting from the initial perfect lattice configuration, the system was relaxed for at least $5 \times 10^4 h = 100\tau$. Following this equilibration period, 2000 configurations were sampled during the sampling time $t_S = 10^5 h = 2000\Delta t \approx 200\tau$ at equal time intervals of $\Delta t = 50h \approx 0.1\tau$. Longer simulation times were used to collect relaxation data for selected densities close to the crystalline state. For each saved configuration, the characteristics of each particle's immediate environment (see below) were calculated, and configurations were visualized with particles' colors, depending on their environmental characteristics. For the isotherm $T = 0.7$, the phase diagram in Figure 1 suggests the liquidus density of $\rho_L = 0.82$ and the solidus density $\rho_S = 0.88$. These values were found[2,38] from thermodynamic data. We use these densities merely to indicat the melting range of densities.

3. Fluctuations of the Local Order

a. Cage Shapes and Bond Orientations. A cage of a particle is defined as its six nearest neighbors. Cage particles are labeled by an index $a = 1, ..., 6$. In the zero-temperature crystal, each particle is surrounded by a perfectly hexagonal cage. When the temperature increases, instantaneous shapes of cages increasingly deviate from this ideal shape. To characterize the shape and orientation of a cage, one can use bond orientation order parameters $Q_n(r)$, $n = 1, 2, 3, ...$, defined as[1]

$$Q_n(r) = \frac{1}{6}\sum_{a=1}^{6} \mathrm{e}^{-ni\varphi^{(a)}} \quad (2)$$

where $\varphi^{(a)}(r)$ is the angle between the x-axis and the direction of the vector connecting the cage center r and the cage particle labeled a. Following refs 39, 40, and 42, we use in this paper the order parameters

$$Q_{(k)}(r) = \frac{1}{6}\sum_{a=1}^{6} Y_{6,k}[\pi/2, \varphi^{(a)}(r)] \qquad k = -6, -5, ..., 6 \quad (3)$$

The shape of a cage is characterized by the shape invariant $Q > 0$

$$Q^2(r) = \frac{4\pi}{13}\sum_{k=-6}^{6} \left|Q_{(k)}\right|^2 \quad (4)$$

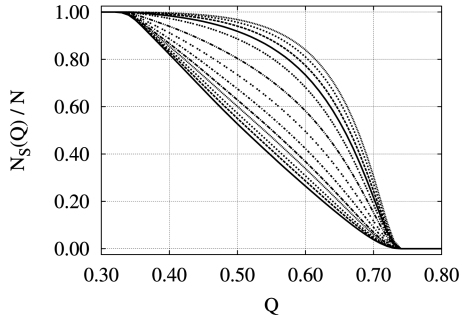

Figure 2. Average fraction of S(Q) particles as a function of Q for reduced densities from 0.78 (bottom) to 0.90 (top) with a step of 0.01.

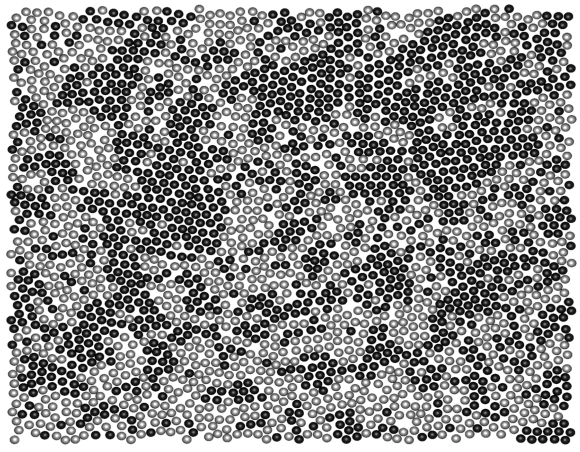

Figure 3. An instantaneous configuration of S(Q) particles (black) and L(Q) particles (gray) in 2500 atom LJ system at $\rho = 0.83$ for $Q = 0.555$.

The value of Q for a perfect hexagon is $Q_{max} \approx 0.7$; with increasing deviation from this ideal shape, the invariant Q decreases. For a particle in the core of a dislocation, the typical values of Q are $0.400 < Q < 0.555$.[40,43] We calculated both $|Q_6|$ and Q for a fluctuating cage and found that to within negligibly small differences, $Q/Q_{max} = |Q_6|$ for $Q_{max} > Q > 0.35$, while for smaller values of $Q < 0.35$, $Q/Q_{max} > |Q_6|$. In the crystal at $\rho > 0.88$, only a small fraction of particles had $Q < 0.555$. Upon moving to lower densities, the fraction of these particles rapidly increased; at $\rho \approx 0.83$, about half of the particles in a typical configuration had $Q < 0.555$.[39,40,42] For a chosen value of the variable parameter Q, we refer to a particle as an S(Q) particle when its cage shape parameter is larger than Q; otherwise, the particle is L(Q). The average fraction $N_S(Q)$ of S(Q) particles as a function of Q for different densities ρ is plotted in Figure 2. Figure 2 is in good agreement with data reported in ref 40.

b. Crystallites and Amorphous Clusters. To visualize S(Q) and L(Q) particles in a given configuration, we colored S(Q) particles black and L(Q) particles gray. Using this convention, a typical configuration at $\rho = 0.83$ is presented in Figure 3. In all sampled configurations, S(Q) and L(Q) particles form clusters. For $Q = 0.555$, at densities ρ in the melting range, all sampled configurations represented a mosaic of differently ordered (and thus colored) clusters. S(Q) particles formed well-packed crystallites having all cages clearly hexagonal while L(Q) particles aggregated into more amorphous clusters with the packing density substantially lower than that in crystallites. Here, crystallites are defined as compact clusters of S(Q) particles for $Q = 0.555$. Using the Burgers mapping procedure,[43] a crystallite can be unambiguously mapped (superimposed) without violations of nearest-neighbors relationships onto a compact and single-connected region of an ideal lattice, and with only small deviations of particles' positions in the crystallite from the sites of this ideal lattice. Orientations of all cages in a crystallite are almost parallel. The typical number of particles in a crystallite was 25−50 particles.

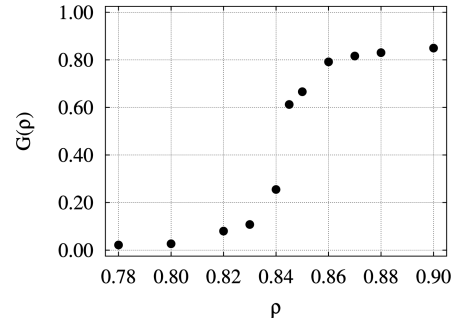

Figure 4. Global orientation order parameter $G(\rho)$ as a function of density ρ.

The particle density in crystallites was higher than the average density ρ of the system. At $\rho = 0.83$, the average distance between nearest neighbors in crystallites was $\langle r_S \rangle = 1.17$, while in amorphous regions, it was $\langle r_L \rangle = 1.23$. A decrease $\delta\rho$ in the average density $\rho = N/V$ resulted in a much smaller decrease $\delta\rho_{cr}$ of the density ρ_{cr} inside of the crystallites, with $\delta\rho_{cr}/\rho_{cr} < (1/2)\delta\rho/\rho$.

At $\rho = 0.90$, there were no amorphous clusters. The fraction of particles in amorphous regions rapidly increased with decreasing average density. At $\rho = 0.84$, amorphous regions (clusters) between crystallites had about the same sizes as crystallites, and about half of the system was in amorphous (and in crystalline) clusters. At smaller densities $\rho < 0.84$, amorphous regions tended to aggregate in larger amorphous regions. Mapping particles of an amorphous cluster onto an ideal lattice appeared ambiguous. Information, described in the next sections about the history of the particles' positions was helpful in diminishing this ambiguity.

In the range of $\rho = 0.83-0.85$, the global orientation order of the system changed dramatically. We defined the global orientation order parameter as

$$G(\rho) = \left| \frac{1}{N_{S(0.555)}} \left[\sum_{\text{all S (0.555) particles}} Q_6(r) \right] \right| \qquad (5)$$

where the sum runs over S(Q) particles only and $Q = 0.555$. This definition excludes L(Q) particles because the orientation of the cage for an L(Q) particle is not a meaningful characteristic. Between $\rho = 0.85$ and 0.83, the finite system rapidly changed from an orientationally ordered to a disordered liquid (see Figure 4). The disorder at smaller densities cannot be explained by the decrease in the number of S(Q) particles; eq 5 compensates for this change. Figure 2 shows that the number of S(Q) particles had not changed as significantly as G. Then, the increased disorder was due to the decreased correlation between orientations of crystallites; at $\rho < 0.83$, orientations of cages were correlated inside of the crystallites but not between different crystallites separated at distances more than a crystallite size, while at densities of $\rho > 0.85$, cage orientations correlated, with only small fluctuations, in the entire system.

c. Dynamics of the Mosaic. The crystallites and amorphous clusters appeared to be short-living; each particle randomly switched between S(Q) and L(Q) at a time of only few in-cage oscillations. However, the crystallites−amorphous clusters

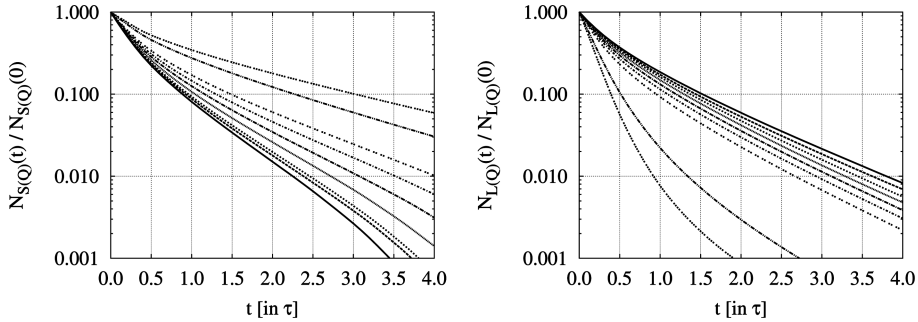

Figure 5. Average fraction of S(Q) particles (left) and L(Q) particles (right), with $Q = 0.555$ continuously remaining S(Q) and L(Q) for time t. *D*ensity (from bottom to top) $\rho = 0.78$, ..., 0.84, 0.86, and 0.88.

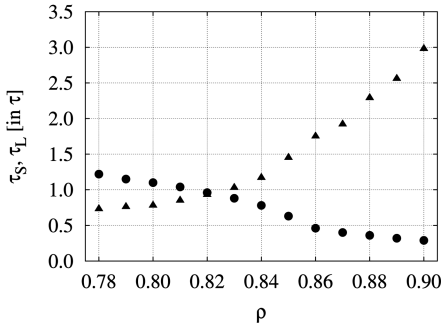

Figure 6. Plot of decay times τ_S (triangles) and τ_L (circles) as function of density ρ.

mosaic existed in all sampled frames, with small fluctuations of the instant numbers of S(Q) and L(Q) particles. The dynamics of mosaic may be described as a fast melting−crystallization oscillatory process. Analysis of configurations sampled at small time intervals reveals that the $S \leftrightarrow L$ "switches" may be described as fast motions of crystallite boundaries; therefore, particles in the middle of larger crystallites have the largest S(Q) lifetimes. Figure 5 gives a logarithmic plot of the average number $N_{S(Q)}(t)$ of S(Q) particles remaining S(Q) continuously (in all configurations sampled) during time t and the average number $N_{L(Q)}(t)$ of L(Q) particles continuously remaining L(Q) for a time t. The decay of $N_{S(Q)}(t)$ and $N_{L(Q)}(t)$ is nonexponential, with two distinctly different slopes at short and longer times. The decay times τ_S and τ_L, defined by the short-time part of the decay of S(Q) and L(Q) correspondingly, are shown in Figure 6. With increasing density in the range of $\rho = 0.82-0.88$, τ_S increased while τ_L decreased, but both times remained on the same order as the cage vibration period τ. The dependence of the mosaic picture on the size of the system is discussed in the Supporting Information.

d. Nearest-Neighbor Changes. Fast changes in the crystallites−amorphous clusters mosaic were in contrast to long lifetimes of the particles' cages for densities $\rho > 0.80$; for times much larger than τ, most of the particles retained the same six nearest neighbors. In a 2D system, the list $P_{nn}(r)$ of six nearest neighbors (nn) of a particle at point r is a local characteristic; for 3D systems, a similar characteristic for a LJ system is the list of 12 nearest neighbors. For more complex systems, the number of particles in the cage may differ. The nn lists are conserved by small displacements; a change in an nn list indicates a particles rearrangement in the system. Physical particles are indistinguishable; therefore, an exchange of particles' positions does not change the physical configuration. In computer simulations, however, each particle is assigned a unique identifier, and the set $\{P_{nn}(r^{(a)})\}$, $a = 1$, ..., N, of nn lists plays the role of a global topological order parameter for the system. A moving point-like defect (vacancy, dislocation) produces a chain of rearrangements and of nn lists along the path of the defect.

We used nn lists as dynamic variables $P_{nn}(r,t)$ and visualized nn changes by changing the color of particles when their nn lists changed. This visualization revealed that most of nn changes are short-lived; a rapid return to the initial nn list signals that the short-time event is not a rearrangement but rather an artifact of our (metric) definition of a cage as six nearest neighbors. However, these short-lived nn changes were only part of all nn changes. When sampled configurations were viewed as a movie, long-lived nn changes mostly appeared as traces of randomly moving defects. These rearrangement changes remained for times much longer than the period of in-cage vibrations, indicating that an energy barrier was passed and the system arrived at a new, relatively stable local nn configuration.

To separate short-time and long-time changes, we memorized the nn lists at a time t' and then changed the color for particles changing their nn lists, either keeping this new color for the rest of the run or removing the marking when the nn -list returned to its initial state. The first method leaves unmarked-only particles, keeping their nn lists continuously in all sampled intermediate configurations. The second method marks only particles that have their nn list at time t different from that memorized. The average number $N_{nn,cont}(t)$ of particles continuously keeping their nn lists for a time t decayed much faster than the average number $N_{nn}(t)$ of particles having the same nn lists at times t' and $t' + t$. For densities of $\rho > 0.82$, the lifetimes of nn lists were much larger than the characteristic time $\sim\tau$ of the mosaic changes.

An exponential fit of the data for $N_{nn}(t)$ shows deviations from a single-exponential decay and an increase of differences between runs at same density for increased density. To characterize the relaxation rate, we defined the half-decay times θ_{nn} and $\theta_{nn,cont}$ as times when the corresponding numbers became one-half of their initial values for, respectively, both $N_{nn}(t)$ and $N_{nn,cont}(t)$. With increasing density, both $\theta_{nn,cont}$ and θ_{nn} significantly increased (Figure 7). The time $\theta_{nn,cont}$ was always smaller than the time θ_{nn}; with increasing densities, the ratio $\theta_{nn}/\theta_{nn,cont}$ rapidly increased. For $\rho > 0.86$, θ_{nn} became too large for the 200τ simulation time, and to estimate θ_{nn}, 10- or 100-times longer simulations have been performed. In the long-time simulations reported in refs 35 and 36, a temperature step resulted in a density jump only after a time delay of about the same order of magnitude as $\theta_{nn}(t)$ for $\rho = 0.87$.

For separate runs at the same density, plots for $N_{nn}(t)$ were qualitatively similar but differed in details. The rate of the decay featured sudden changes that we associated with appearances or disappearances of defects. The difference in the plots between different runs increased with increasing density ρ and, cor-

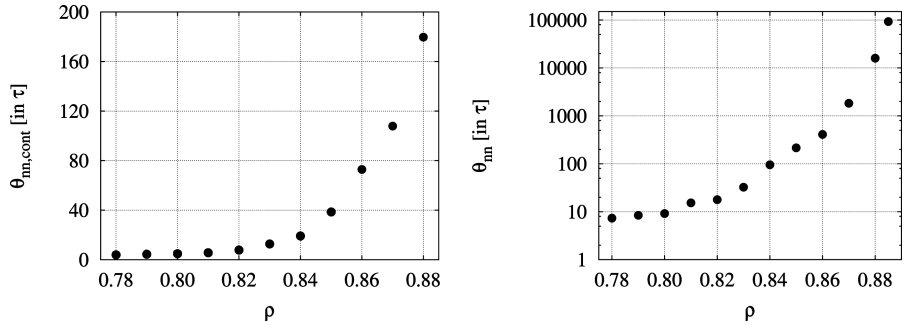

Figure 7. Plots of half-decay times $\theta_{nn,cont}$ (left) and θ_{nn} (right) as a function of density.

respondingly, decreasing defect number. For $\rho > 0.88$, the decrease of $N_{nn}(t)$ became practically undetectable at simulation times of $\sim 200\tau$, and the simulation time needed for estimating θ_{nn} had to be increased many times.

We note that the mosaic picture and especially the nonexponential long-time relaxation of the nn topologic characteristics strongly resemble the picture usually supposed[44] in glass formers near glass transition, with crystallites playing the role of solid-like clusters and amorphous regions playing the role of liquid-like clusters. However, in glass-forming liquids, the lifetime of the solid-like−liquid-like mosaic is supposed to be much larger than particle vibration period. Unlike glass formers, the low-temperature state of our 2D system is long-range-ordered without frustration. Macroscopic stress relaxation and hydrodynamic flow always involve changes in the nearest neighbors of particles. The lifetime $\theta_{nn}(t)$ of the local topological order in a system plays the role of the smallest length scale relaxation time. The larger-scale structure relaxation can take a much longer time for sampling a representative ensemble of structures, including the positions and number of defects. The typical feature of glass formers is that the glass is supercooled faster than the structure can equilibrate, and thus, glass is more disordered than the equilibrium system at the same thermodynamic parameters. The initial state of our simulations is an ideal crystal. For very large θ_{nn}, the system at the observation time remains rather overordered. Nevertheless, in both cases, the nonequilibrium order is frozen in, and a slow relaxation takes place in this nonequilibrium state.

4. Discussion and Interpretation of the Results

a. Mosaic Picture. We assume, based on the results of simulations in refs 35 and 36, that the phase transition in a macroscopic 2D LJ system is discontinuous. One expects then that under constant volume conditions at the phase transition, the system consists of two coexisting phases separated by an interface. However, in the $N = 2500$ system, we observed no detectable phase separation on the length scale larger than the crystallites size. To control the stability of the picture, we performed 10- and 100-times longer simulations at selected density values in the transition range, but even for these long times, no coarsening or phase separation was observed. The most likely explanation here is that the phase-separating interface is too wide to fit into the 50×50 system. Suggesting a large width of the interface can also explain the large size effects in the value of the phase-transition temperature reported in ref 18. One expects that in a system that is too small to host the interface and thus a critical nucleus of a new phase, the local properties of configurations are similar to those of small parts inside of the wide interface existing in large systems. The phase diagram in Figure 1 is an extrapolation of the data obtained in systems about the size or even smaller than the $N = 2500$ system.

As described, in the crystal at $\rho > 0.88$ and in the liquid at $\rho < 0.80$, density fluctuations in compact clusters of $n \approx 25$ particles were small and did not change the local structure. In the range of $\rho = 0.82-0.88$, and especially $\rho = 0.83-0.85$, these fluctuations were large and coupled with structure changes; small regions of $\sim 20-50$ particles fluctuated between crystalline and amorphous packing. As a dynamic variable, the volume $V = n/\rho$ of a compact cluster of $n \approx 25$ particles is only one of $2n \approx 50$ internal degrees of freedom of the cluster; therefore, for each δV, there is an ensemble of configurations. Then, at least qualitatively, the cluster can be described using thermodynamics.

We suggest that the competition between attraction and repulsion in the LJ interaction enhanced the density and structure fluctuations represented by the mosaic picture. Due to this attraction, the absolute minimum of the potential energy of the 2D LJ system corresponds to the final density $\rho_{gs} \approx 0.92$; for a system of classical particles, this is the density of the $T = 0$ crystal at the gas−crystal coexistence point (see Figure 1) where the pressure is $P = 0$. In a finite system, ρ_{gs} depends on the size of the system. Along the crystal−gas coexistence line, the pressure increases, but the density of the crystal decreases. Above the triple-point temperature, along the crystal−liquid transition line, the density of the crystal increases, but for $T < T0 \approx 1$, it remains below ρ_{gs}; therefore, the crystal is stretched relative to its absolute minimum of the energy state. For a density below ρ_{gs}, a fluctuation increasing the density and also the crystalline order in the cluster increases the potential energy but decreases the entropy; a fluctuation that decreases the density results in an increase of energy and of entropy. We note that due to the LJ attraction, a density fluctuation in a stretched state has coinciding signs of energy and entropy changes, and these changes at least partially compensate each other in the free energy $\delta F = \delta U - T\delta S$ of the fluctuation.

Applying thermodynamic methods,[45] one writes the free energy δF of a fluctuation in an n-particle cluster fluctuating at constant T and P as $\delta F = (k_{loc}/2V)(\delta V)^2 +$ (terms of higher order in δV), where δV is the change in volume and the local moduli are $k_{loc} = -V(\partial P_{loc}/\partial V)_T$ and $P_{loc} = -(\partial F \partial V)_T$. The change in the density is $\delta\rho = -\rho(\delta V/V)$. The average magnitude $\langle \delta V^2 \rangle$, $\langle \delta \rho^2 \rangle$ of fluctuations is determined by the condition that for these magnitudes, $\delta F \approx T$. When k_{loc} is large, one neglects the higher than quadratic order terms in δF and obtains $\langle \delta V^2 \rangle \approx VT/k_{loc}$, $\langle \delta \rho^2 \rangle \approx \rho^2 T/(Vk_{loc})$. The assumed compensation of energy and entropy contributions to δF diminishes the local modulus k_{loc} and thus leads to an increase in density fluctuations in small clusters. One expects maximum compensation and for the minimal value of k_{loc} to be at some density between liquidus and solidus.

The rather hand-waving qualitative arguments about the energy−entropy compensation need a quantitative verification. To this end, we note that van der Waals loops at melting have been observed in the 2D LJ and other 2D systems, but these

loops do not necessarily signal a discontinuous transition.[48] Our calculations of the pressure in small periodic systems of 5×5, 7×7, 10×10, and 15×15 particles found the bulk modulus $k = -V(\partial P/\partial V)_T$ to be very small or negative in a narrow range of densities. In particular, at $T = 0.7$, this range was inside of the melting range $\rho = 0.82-0.88$. At higher temperatures, this range shifted to higher densities approximately parallel to the solidus line in Figure 1 and narrowed; the extrapolation is that above some temperature $T_0 \approx 1$, the modulus becomes positive and large for all densities.

In models of phase transitions between phases with differing local structures (see ref 34), the increase in fluctuations in small clusters, indicating competing local structures, is only a necessary condition for a discontinuous transition. The changes may be continuous as in the transition from liquid to gas above the critical point; the appearance of a singularity assumes special features of the interaction of fluctuations in different clusters.

b. Interaction of Amorphyzation Melting with the Dislocation−Unbinding Mechanism. In the $N = 2500$ system at $T = 0.7$, the local order changed from crystalline to amorphous in the melting range of densities of $\rho = 0.82-0.88$; in the same density range, the orientation order in the system disappeared. In large systems of refs 35 and 36, correlation of cage orientations at the solidus density algebraically decayed at large distances, as predicted in the dislocation−unbinding theory for a close vicinity to the unbinding transition. In contrast to this behavior, in a repulsion-only system,[37] the transition from a usual to hexatic liquid was detected at a temperature close to but higher than that of crystallization. We note that amorphyzation melting and dislocation−unbinding are scenarios for different phase transitions, and corresponding phase-transition temperatures for these scenarios are expected to be different. The simulation data[25,28,35−37] are consistent with the assumption that for hard disks and repulsion-only systems, the unbinding temperature T_{un} is slightly below the amorphyzation transition temperature T_{am}, while for the LJ system at $T < T_0$, it is slightly above T_{am}. We suggest that this is due to the attraction part of the LJ system.

Phase transitions between phases differing in local structure are known in many systems.[34,39,46,47,49−55] The list of these transitions includes polymorphous transitions in crystals[49] and liquid−liquid phase transitions with a change in local structure (polyamorphous transitions)[50−55] a rather general model for these transitions was studied in refs 34 and 35. Such a transition is primarily a finite-scale phenomenon not implying a special long-range order, although the long-range order may change when the local structure changes. In application to the 2D LJ system, the term "local" refers to the crystallites length scale, and the observed transition is between the crystalline and amorphous local structures. The difference between a crystal and a hexatic liquid and hexatic and usual liquids cannot be reliably recognized in a finite and rather small system, although the amorphyzation is more detectable because a system of $N = 2500$ particles includes ~100 nonoverlapping clusters of the crystallites size (~25 particles). Our identification of the phase transition as discontinuous relies on simulations of larger systems;[35,36] our data about the $N = 2500$ system cannot discriminate between the crystal and the hexatic liquid; the hexatic to normal liquid transition is also an amorphyzation transition. What our data show is the interaction between the unbinding and amorphyzation mechanisms due to almost coinciding transition temperatures.

In the BKTNHY theory,[6,7] the unbinding temperature T_{un} is proportional to the shear modulus μ characterizing the shear rigidity on the initial length scale R_0 of the theory, $T_{un}(\mu) = \gamma\mu_{un}$. Simulation data[1] indicate that R_0 is on the order of the size of the $N = 2500$ system.The amorphyzation transition in a macroscopic system results in a jump of μ from the value μ_{cr} in the crystal to a much smaller value μ in the liquid; μ in the liquid differs from zero because in a cluster of the size R_0, some order may remain. The apparent unbinding temperature defined as $T_{un}(T,\rho) = \gamma\mu(T,\rho)$ depends on density and temperature. When $T_{un}(T_{am},\rho) > T_{am}$, the system at the amorphyzation transition is crystalline, and the orientation long-range order disappears in the course of the amorphyzation transition from the crystalline to amorphous phase. When $T_{un}(T,\rho) = \gamma\mu_{un}$ at a temperature $T < T_{am}$, the unbinding transition takes place before amorphyzation.

Simulation data[25,28,35−37] indicate that for all systems studied, the unbinding and amophyzation temperatures nearly coincide; therefore, if the equilibrium hexatic liquid exists, it only exists in a narrow range of temperatures. In 2D and 3D systems at amorphyzation melting, the mean-square displacements reach the level given by the Lindemann criterion. A similar criterion can be formulated in terms of cage fluctuations; as shown in ref 40 and in the above sections, both the onset of amorphyzation and disappearance of orientation order take place at the level of cage fluctuations when $Q < 0.555$ in about half of the particles. Then, the crystal close to melting is also close to the amorphyzation transition, and amorphyzation premelting is expected to decrease $\mu(T,\rho)$ compared to its low-temperature values. For close transition temperatures of the two transitions, this effect can be large; one can say that in the vicinity of the amorphyzation transition, the apparent unbinding temperature rapidly moves toward the slowly increasing temperature T. The two temperatures meet above[37] or below[35,36] but close to the amorphyzation temperature T_{am}.

For the case when $T_{un} > T_{am}$, a large isobaric system can be overheated and become metastable. The metastable crystal is later destroyed by nucleation and growth of the liquid phase; for some size of the system, this process can be oscillatory.[56] The density of the overheated crystal is lower than in the solidus state. From the data presented in refs 35 and 36, the lifetime of the overheated crystal was about the time of significant changes of particle near neighbors, much larger than the relaxation time of the mosaic. We suggest that the decrease in density below the solidus value lead to a smaller shear modulus μ; therefore, the metastable crystal reached the unbinding conditions.

5. Conclusion

Visualization of the local order and disorder in a 2D LJ system at $T = 0.7$ and density in the transition range of $0.86-0.82$ revealed that a typical configuration is a mosaic of small crystalline and amorphous clusters. When the density was diminished over the transition range, the fraction of amorphous clusters rapidly increased from small to large; simultaneously, the orientation order diminished and then vanished. Our observations suggest an amorphyzation transition underlying these structural changes; due to the small size of the system, we can not distinguish if this transition happens in the crystal or a hexatic liquid. Structural changes near the amorphyzation transition support the assumption that in a large-size system, amorphyzation forces the long-range orientation order to disappear by diminishing the shear rigidity.

Acknowledgment. This work was supported by the Non-equilibrium Energy Research Center (NERC), which is an Energy Frontier Research Center funded by the U.S. Department

of Energy, Office of Science, Office of Basic Energy Sciences under Award Number DE-SC0000989.

Supporting Information Available: Data and discussion of the size dependence of the mosaic picture. This material is available free of charge via the Internet at http://pubs.acs.org.

References and Notes

(1) Strandburg, K. J. *Rev. Mod. Phys.* **1988**, *60*, 161–207.
(2) Glaser, M. A.; Clark, N. A. *Adv. Chem. Phys.* **1993**, *83*, 543–709.
(3) Patrykiejew, A.; Sokolowski, S.; Binder, K. *Surf. Sci. Rep.* **2000**, *37*, 209–344.
(4) (a) Berezinskii, L. *Sov. Phys. JETP.* **1971**, *32*, 493–501. (b) Berezinskii, L. *Sov. Phys. JETP* **1972**, *34*, 610–619.
(5) Kosterlitz, M.; Thouless, P. J. *J. Phys. C* **1973**, *6*, 1181–1203.
(6) Halperin, I.; Nelson, D. R. *Phys. Rev. Lett.* **1978**, *41*, 121–124.
(7) Nelson, D. R.; Halperin, B. I. *Phys. Rev. B* **1979**, *19*, 2457–2094.
(8) (a) Young, A. P. *J. Phys. C* **1978**, *11*, L453–L455. (b) Young, A. P. *Phys. Rev. B* **1979**, *19*, 1855–1866.
(9) Monson, P. A.; Steele, W. A.; Henderson, D. *J. Chem. Phys.* **1981**, *74*, 6431–6439.
(10) Barker, J. A.; Henderson, D.; Abraham, F. F. *Physica A* **1981**, *106*, 226–238.
(11) Klein, J. R.; Cole, M. W. *Faraday Discuss. Chem. Soc.* **1985**, *80*, 71–78.
(12) (a) Cuadros, F.; Mulero, A. *Chem. Phys.* **1993**, *177*, 53–60. (b) Cuadroa, F.; Mulero, A. *J. Phys. Chem.* **1995**, *99*, 419–423.
(13) Zeng, X. C. *J. Chem. Phys.* **1996**, *104*, 2699–2704.
(14) Alder, B. J.; Wainwright, T. E. *Phys. Rev.* **1962**, *127*, 359–368.
(15) Hoover, W. G.; Alder, B. J. *J. Chem. Phys.* **1967**, *46*, 686–693.
(16) Hoover, W. G.; Ree, F. H. *J. Chem. Phys.* **1968**, *49*, 3609–3918.
(17) Wood, W. W. *J. Chem. Phys.* **1970**, *52*, 729–742.
(18) Strandburg, K. J.; Zollweg, J. A.; Chester, G. V. *Phys. Rev. B* **1984**, *30*, 2755–2759.
(19) Zollweg, J. A.; Chester, G. V.; Leung, P. W. *Phys. Rev. B* **1989**, *39*, 9518–9530.
(20) Fraser, D. P.; Zuckermann, M. J.; Mouritsen, O. G. *Phys. Rev. A* **1990**, *42*, 3186–3195.
(21) Zollweg, J. A.; Chester, G. V. *Phys. Rev. B* **1992**, *46*, 11187–11189.
(22) Lee, J.; Strandburg, K. J. *Phys. Rev. B* **1992**, *46*, 11190–11193.
(23) Weber, H.; Marx, D. *Europhys. Lett.* **1994**, *27*, 593–598.
(24) Weber, H.; Marx, D.; Binder, K. *Phys. Rev. B* **1995**, *51*, 14636–14651.
(25) (a) Fernandez, J. F.; Alonso, J. J.; Stankiewicz, J. *Phys. Rev. Lett.* **1995**, *75*, 3477–3480. (b) Fernandez, J. F.; Alonso, J. J.; Stankiewicz, J. *Phys. Rev. Lett.* **1997**, *78*, 399–399. (c) Fernandez, J. F.; Alonso, J. J.; Stankiewicz, J. *Phys. Rev. E* **1997**, *55*, 750–764.
(26) Weber, H.; Marx, D. *Phys. Rev. Lett.* **1997**, *78*, 398–398.
(27) Mitus, A. C.; Weber, H.; Marx, D. *Phys. Rev. E* **1997**, *55*, 6855–6859.
(28) (a) Jaster, A. *Phys. Rev. E* **1999**, *59*, 2594–2602. (b) Jaster, A. *Europhys. Lett.* **1998**, *42*, 277–281.
(29) Sengupta, S.; Nielaba, P.; Binder, K. *Phys. Rev. E* **2000**, *61*, 6294–6301.
(30) Binder, K.; Sengupta, S.; Nielaba, P. *J. Phys.: Condens. Matter* **2002**, *14*, 2323–2333.
(31) Phillips, J. M.; Bruch, L. W.; Murphy, R. D. *J. Chem. Phys.* **1981**, *75*, 5097–5109.
(32) Udink, C.; van der Elsken, J. *Phys. Rev. B* **1987**, *35*, 279–283.
(33) Chui, S. T. *Phys. Rev. B* **1983**, *28*, 178–194.
(34) Patashinski, A. Z.; Ratner, M. A. *J. Chem. Phys.* **1997**, *106*, 7249–7256.
(35) Chen, K.; Kaplan, T.; Mostroller, M. *Phys. Rev. Lett.* **1995**, *74*, 4019–4022.
(36) Chen, K.; Kaplan, T.; Mostroller, M. *Computer Simulation Studies in Condensed-Matter Physics IX*. Proceedings of the Ninth Workshop, Athens, GA, U.S.A., March 4−9, 1996; Springer: New York, 1996.
(37) (a) Bagchi, K.; Andersen, H. C.; Swope, W. *Phys. Rev. E* **1996**, *53*, 3794–3803. (b) Bagchi, K.; Andersen, H. C.; Swope, W. *Phys. Rev. Lett.* **1996**, *76*, 255–258.
(38) Abraham, F. F. *Phys. Rep.* **1981**, *80*, 340–374.
(39) Patashinski, A. Z.; Mitus, A. C.; Ratner, M. A. *Phys. Rep.* **1997**, *288*, 409–434.
(40) Mitus, A. C.; Patashinski, A. Z.; Patrykiejew, A.; Sokolowski, S. *Phys. Rev. B* **2002**, *66*, 184202/1–184202/12.
(41) Allen, M. P.; Tildesley, D. J. *Computer Simulations of Liquids*; Clarendon Press: Oxford, U.K., 1987.
(42) Mitus, A. C.; Patashinskii, A. Z.; Sokolowski, S. *Physica A* **1991**, *174*, 244–271.
(43) Landau, L. D.; Lifshitz, E. M. *Theory of Elasticity. Course in Theoretical Physics. Vol. 7*; Pergamon: Oxford, U.K., 1970.
(44) Tarjus, G.; Kivelson, S. A.; Nussinov, Z.; Viot, P. *J. Phys.: Condens. Matter* **2005**, *17*, R1143–R1182.
(45) Landau, L. D.; Lifshitz, E. M. *Statistical Physics. Course in Theoretical Physics. Vol. 5*: Pergamon: Oxford, U.K., 1961.
(46) (a) Stillinger, F. H.; Weber, T. A. *Phys. Rev. A* **1982**, *25*, 978–989. (b) Stillinger, F. H.; Weber, T. A. *Phys. Rev. A* **1983**, *28*, 2408–2416. (c) Stililnger, F. H.; Weber, T. A. *Science* **1984**, *225*, 983–989.
(47) LaViolette, R. A.; Stillinger, F. H. *J. Chem. Phys.* **1985**, *83*, 4079–4085.
(48) Alonso, J. J.; Fernandez, J. F. *Phys. Rev. E* **1999**, *59*, 2659–2663.
(49) Bernstein, J. *Polymorphism in Molecular Crystals*: University Press, Oxford, New York, 2008.
(50) Mitus, A. C.; Patashinskii, A. Z.; Shumilo, B. I. *Phys. Lett. A* **1985**, *113*, 41–44.
(51) Mitus, A. C.; Patashinskii, A. Z. *Acta Phys. Pol., A* **1988**, *47*, 779–787.
(52) (a) Brazhkin, V. V.; Voloshin, R. N.; Popova, S. V. *JETP Lett* **1989**, *50*, 424–428. (b) Brazhkin, V. V.; Voloshin, R. N.; Popova, S. V. *Phys. Lett. A* **992**, *166*, 383–388.
(53) (a) Brazhkin, V. V.; Voloshin, R. N.; Popova, S. V.; Umnov, A. G. *J. Phys.: Condens. Matter* **1992**, *4*, 1419–1429. (b) Brazhkin, V. V.; Voloshin, R. N.; Popova, S. V.; Umnov, A. G. *Phys. Lett. A* **1991**, *154*, 413–417.
(54) Sciortino, F.; Poole, P. H.; Essmann, U.; Stanley, H. E. *Phys. Rev. E* **1979**, *55*, 727–738.
(55) Harrington, S.; Zhang, R.; Poole, P. H.; Sciortino, F.; Stanley, H. E. *Phys. Rev. Lett.* **1997**, *78*, 2409–2413.
(56) Patashinski, A.; Ratner, M. *Phys. Rev. E* **2008**, *78*, 041106/1–041106/7.

JP1069412